

Intervallence Transfer in Mixed-Metal Dimers of Ruthenium and Osmium: Relationship between Redox Asymmetry and Intervallence-Transfer Absorption Band Energy

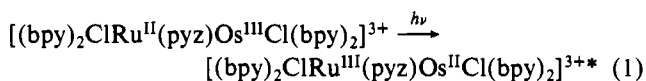
KENNETH A. GOLDSBY and THOMAS J. MEYER*

Received September 19, 1983

The symmetrical Ru-Ru and mixed-metal Ru-Os mixed-valence dimers $[(\text{bpy})_2\text{ClRu}(\text{B})\text{MCl}(\text{bpy})_2]^{3+}$, $[(\text{bpy})_2\text{Ru}(\text{bpm})\text{M}(\text{bpy})_2]^{3+}$, and $[(\text{bpy})_2\text{ClRu}(\text{pyzc})\text{M}(\text{bpy})_2]^{3+}$ (bpy = 2,2'-bipyridine; B = pyrazine, 4,4'-bipyridine; bpm = 2,2'-bipyrimidine; pyzc = 2-pyrazinecarboxylate anion; M = Ru, Os) all display broad, low-energy intervalence transfer (IT) absorption bands which have the properties expected for optically induced electron transfer between weakly coupled metal centers. For the mixed-metal dimers, the IT bands are observed at a systematically higher energy than IT bands in analogous $\text{Ru}^{\text{II}}\text{-Ru}^{\text{III}}$ dimers consistent with the redox asymmetry in the dimers and the equation $E_{\text{op}} = \chi + \Delta E$, where E_{op} is the energy of the optical transition, χ is the vibrational trapping or reorganizational energy, and ΔE is the internal energy change. IT bandwidths at half-height ($\Delta\bar{\nu}_{1/2}$) for analogous pairs of Ru-Ru and Ru-Os dimers are similar as predicted by the Hush equation ($\Delta\bar{\nu}_{1/2} = [16(\ln 2)\chi k_{\text{B}}T]^{1/2}$), suggesting that vibrational reorganizational energies are comparable for the two types of dimers. The increase in E_{op} for the unsymmetrical dimers can be accounted for quantitatively in terms of the internal energy change ΔE . Given the similarities in molecular volumes between the Ru and Os sites, a thermodynamic analysis shows that ΔE can be calculated from reduction potential data for the Ru(III/II) and Os(III/II) couples in the dimers. As calculated from IT band intensities, the extent of delocalization between M(II) and M(III) sites in the mixed-valence dimers, α^2 , is comparable for the $\text{Ru}^{\text{II}}\text{-Ru}^{\text{III}}$ and $\text{Ru}^{\text{II}}\text{-Os}^{\text{III}}$ dimers, suggesting that electronic coupling between metal centers is dominated by Ru^{II} mixing with the bridging ligand.

Introduction

Assuming weak electronic coupling and the classical limit, Hush has derived equations that describe the properties of intervalence transfer (IT) or metal-to-metal charge transfer (MMCT) absorption bands, e.g., eq 1. Some of the Hush



equations are shown in eq 2-4,¹ where E_{op} is the optical band

$$E_{\text{op}} = \Delta E + \chi_i + \chi_o \quad (2a)$$


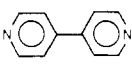
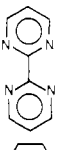
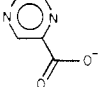
$$= \Delta E + \chi_i + \frac{1}{2} \left(\frac{1}{D_{\text{op}}} - \frac{1}{D_s} \right) \int (\bar{D}_f - \bar{D}_i)^2 dV \quad (2b)$$

$$\Delta\bar{\nu}_{1/2} = [16(\ln 2)k_{\text{B}}T(E_{\text{op}} - \Delta E)]^{1/2} \quad (3)$$

$$E_{\text{th}} = \frac{(\Delta E + \chi_i + \chi_o)^2}{4(\chi_i + \chi_o)} \quad (4)$$

energy at λ_{max} , ΔE is the internal energy difference between the two oxidation-state isomers, χ_i and χ_o are the classical inner-sphere and outer-sphere vibrational reorganization or trapping energies, D_{op} and D_s are the optical and static dielectric constants of the medium ($D_{\text{op}} = n^2$, where n is the index of refraction of the medium), \bar{D}_i and \bar{D}_f are the electric displacement vectors of the mixed-valence compound before and after electron transfer corresponding to the hypothetical charge distributions in the absence of the medium, $\Delta\bar{\nu}_{1/2}$ is the bandwidth at half-height for the IT band at temperature T , and E_{th} is the classical barrier to thermal electron transfer. The validity of the Hush equations is limited to cases where contributions from high-frequency vibrations are negligible; however, they have been useful in accounting for bandwidths and solvent dependences of IT bands,²⁻⁶ and eq 4 has been used

Table I. Bridging Ligands Used

name	structure	abbrev
pyrazine		pyz
4,4'-bipyridine		4,4'-bpy
2,2'-bipyrimidine		bpm
2-pyrazinecarboxylate		pyzc

to interrelate intervalence transfer and the analogous thermal electron transfer process.^{7,8} In contrast, the relationship between E_{op} and ΔE given in eq 2a has proven difficult to verify experimentally for chemical reasons.

Equation 2a predicts that E_{op} should vary linearly with ΔE in the limit that χ_i and χ_o remain unchanged. One approach to testing eq 2a is through a related series of mixed-valence compounds where ΔE is varied through ligand variations. However, such changes can lead to changes in intramolecular vibrations and bond lengths and thus to changes in χ_i , and if molecular dimensions are altered appreciably, to changes in χ_o .

The approach we have taken, the results of which are described here, is to turn to structurally analogous $\text{Ru}^{\text{II}}\text{-Ru}^{\text{III}}$ and mixed-metal $\text{Ru}^{\text{II}}\text{-Os}^{\text{III}}$ dimers based on the bridging

(1) (a) Hush, N. S. *Trans. Faraday Soc.* **1961**, *57*, 557. (b) Hush, N. S. *Prog. Inorg. Chem.* **1967**, *8*, 391. (c) Hush, N. S. *Electrochim. Acta* **1968**, *13*, 1005.
(2) Powers, M. J.; Meyer, T. J. *J. Am. Chem. Soc.* **1980**, *102*, 1289.

(3) (a) Meyer, T. J. *Ann. N.Y. Acad. Sci.* **1978**, *313*, 496. (b) Meyer, T. J. In "Mixed-Valence Compounds"; Brown, D., Ed.; D. Reidel: Dordrecht, The Netherlands, 1980; p 75. (c) Meyer, T. J. In "Mechanistic Aspects of Inorganic Reactions"; Rorabacher, D. B., Endicott, J. F., Eds.; American Chemical Society: Washington, DC, 1982; ACS Symp. Ser. No. 198, p 137.
(4) Taube, H. *Ann. N.Y. Acad. Sci.* **1978**, *313*, 481.
(5) Creutz, C. *Prog. Inorg. Chem.* **1983**, *30*, 1.
(6) Sullivan, B. P.; Curtis, J. C.; Kober, E. M.; Meyer, T. J. *Nouv. J. Chim.* **1980**, *4*, 643.
(7) (a) Curtis, J. C.; Sullivan, B. P.; Meyer, T. J. *Inorg. Chem.* **1980**, *19*, 3833. (b) Curtis, J. C.; Meyer, T. J. *Inorg. Chem.* **1982**, *21*, 1562.
(8) Meyer, T. J. *Chem. Phys. Lett.* **1979**, *64*, 417.

ligands listed in Table I. The dimers were chosen because of the known similarities in ionic radii and metal-ligand bond lengths for related Ru and Os complexes,⁹ since the similarities between metals are expected to minimize variations in χ_i and χ_o .

Experimental Section

Measurements. Near-infrared spectra were recorded on a Cary Model 17 spectrophotometer. Electrochemical measurements were made vs. the saturated sodium chloride calomel electrode (SSCE) at room temperature and are uncorrected for junction potential effects. Burdick & Jackson acetonitrile was employed as the electrochemical solvent and 0.1 M tetrabutylammonium hexafluorophosphate (TBAH) as the electrolyte. Cyclic voltammetry measurements were made with a PAR Model 173 potentiostat for potential control with a Model 175 universal programmer as a sweep generator. The $E_{1/2}$ values from cyclic voltammetry were calculated from half the sum of the E_p values for the anodic and cathodic waves. Differential pulse polarography measurements were made with a PAR Model 174A polarographic analyzer. All cyclic voltammetry and differential pulse polarography measurements were carried out at platinum-bead electrodes. Elemental analyses were performed by Galbraith Laboratories, Inc., Knoxville, TN.

Materials. TBAH, $[(t-C_4H_9)_4]PF_6$, was prepared as described previously¹⁰ and recrystallized from hot acetone/ethanol three times. Burdick & Jackson acetonitrile was used for electrochemical measurements. All other chemicals and solvents were reagent grade and were used without further purification.

Preparations. The complexes *cis*-(bpy)₂RuCl₂·2H₂O,¹¹ [(bpy)₂ClRu(py₂)RuCl(bpy)₂](PF₆)₂, and [(bpy)₂ClRu(4,4'-bpy)-RuCl(bpy)₂](PF₆)₂² were prepared according to previously published procedures. The complexes [(bpy)₂ClOs(4,4'-bpy)]PF₆^{12a} and [(bpy)₂ClRu(py₂)OsCl(bpy)₂](PF₆)₂^{12b} were prepared by the method of Kober. Although *cis*-(bpy)₂OsCl₂ can be prepared by the original procedure of Dwyer et al.,¹³ in reasonable yields, the yields from a modified procedure using ethylene glycol as solvent were typically much better.¹⁴

[(bpy)₂ClRu(4,4'-bpy)OsCl(bpy)₂](PF₆)₂. [(bpy)₂ClOs(4,4'-bpy)]PF₆ (0.105 g, 0.122 mmol) and *cis*-(bpy)₂RuCl₂·2H₂O (0.101 g, 0.194 mmol) were combined in 10 mL of 50% EtOH/H₂O and heated to reflux under Ar while maintaining magnetic stirring. This and subsequent manipulations were carried out under reduced light. After 18 h, LiCl (0.12 g, 2.8 mmol) was added to the reaction mixture, which was then heated at reflux for an additional 2 h. After this time, the reaction mixture was allowed to cool and a solution of NH₄PF₆ (1–2 g) in ~15 mL of H₂O was filtered slowly into the stirring solution, precipitating a purple solid. The solution volume was reduced to approximately one-fourth on a rotary evaporator and placed in a refrigerator overnight. The purple solid was isolated by suction filtration, washed well with H₂O followed by anhydrous diethyl ether, and air-dried for several minutes. The crude dimer was purified by column chromatography. The purple solid was dissolved in a minimum amount of 1:2 CH₃CN/C₆H₅CH₃ and pipetted onto a 4 cm × 11 cm column of alumina packed in the same solvent mixture. Elution with 1:2 CH₃CN/C₆H₅CH₃ gave a purple band of the desired dimer, which was preceded by a burnt orange band and followed by a pink band and a brown band. A dark band remained at the top of the column. Continued elution with 1:2 CH₃CN/C₆H₅CH₃ resulted in removal of the burnt-orange band which was discarded. Gradual enrichment to 1:1 CH₃CN/C₆H₅CH₃ effected removal of the purple band, which was collected and taken to dryness on a rotary evaporator. The dimer was reprecipitated from CH₃CN/Et₂O to give 0.065 g of a purple solid, yield 36%. Anal. Calcd for [(C₁₀H₈N₂)₂ClRu(C₁₀H₈N₂)-OsCl(C₁₀H₈N₂)₂](PF₆)₂·H₂O: C, 41.38; H, 2.92; N, 9.65. Found: C, 41.33; H, 2.99; N, 9.49.

[(bpy)₂Ru(bpm)](PF₆)₂. The synthesis of this complex has been reported elsewhere;^{15,16} however, the following preparation was found to be superior to the literature preparation.

cis-(bpy)₂RuCl₂·2H₂O (0.214 g, 0.411 mmol) and 2,2'-bipyrimidine (0.130 g, 0.821 mmol) were combined in 25 mL of 20% EtOH/H₂O and heated to reflux under Ar while magnetic stirring was maintained. After 5 h, a solution of NH₄PF₆ (1.6 g, 9.8 mmol) in ~10 mL of H₂O was filtered slowly into the warm, stirring reaction mixture. The resulting brick red precipitate was isolated by suction filtration, washed well with cold H₂O, and placed in a vacuum desiccator overnight. The complex was obtained in 93% yield. Anal. Calcd for [(C₁₀H₈N₂)₂Ru(C₈H₆N₄)](PF₆)₂: C, 39.03; H, 2.58; N, 13.01. Found: C, 38.77; H, 2.72; N, 12.88.

[(bpy)₂Ru(bpm)Ru(bpy)₂](PF₆)₄. As with the monomeric analogue, the synthesis of this dimer has appeared elsewhere;^{15,16} however, the following procedure gave a much higher yield. Also, the dimer was obtained analytically pure, eliminating the need for chromatography.

[(bpy)₂Ru(bpm)](PF₆)₂ (0.093 g, 0.108 mmol) and *cis*-(bpy)₂RuCl₂·2H₂O (0.073 g, 0.140 mmol) were combined in 10 mL of 30% EtOH/H₂O and heated at reflux under Ar while magnetic stirring was maintained. After 12, 24, and 36 h, 5 mL of EtOH was added to redissolve caked solid from around the inside walls of the flask. After 48 h, a solution of excess NH₄PF₆ (1–2 g) in 15 mL of H₂O was filtered into the stirring reaction mixture, resulting in the precipitation of a dark green solid. The mixture was transferred to a refrigerator for 1 day, after which the solid was isolated by suction filtration and washed with H₂O until the filtrate came through green. The dimer was dried in a vacuum desiccator overnight; yield 85%. Anal. Calcd for [(C₁₀H₈N₂)₂Ru(C₈H₆N₄)Ru(C₁₀H₈N₂)₂](PF₆)₄: C, 36.84; H, 2.45; N, 10.74. Found: C, 36.75; H, 2.69; N, 10.60.

This dimer can also be prepared in good yield by heating *cis*-(bpy)₂RuCl₂·2H₂O with 1/2 equiv of 2,2'-bipyrimidine in EtOH/H₂O; however, the crude dimer must then be purified by chromatography.

[(bpy)₂Os(bpm)](PF₆)₂. *cis*-(bpy)₂OsCl₂ (0.198 g, 0.345 mmol) and 2,2'-bipyrimidine (0.093 g, 0.587 mmol) were combined in 25 mL of 20% EtOH/H₂O and heated at reflux under Ar for 36 h while magnetic stirring was maintained. After this time, a solution of excess NH₄PF₆ (1–2 g) in ~10 mL of H₂O was filtered slowly into the stirring reaction mixture, yielding a dark green precipitate. After several hours at room temperature, the dark green solid was isolated by suction filtration, washed with H₂O (3 × 10 mL), and placed in a vacuum desiccator overnight. The complex was obtained in 83% yield. Anal. Calcd for [(C₁₀H₈N₂)₂Os(C₈H₆N₄)](PF₆)₂: C, 35.37; H, 2.34; N, 11.79. Found: C, 35.20; H, 2.42; N, 11.58.

[(bpy)₂Ru(bpm)Os(bpy)₂](PF₆)₄. [(bpy)₂Os(bpm)](PF₆)₂ (0.105 g, 0.111 mmol) and *cis*-(bpy)₂RuCl₂·2H₂O (0.299 g, 0.575 mmol) were combined in 20 mL of 20% EtOH/H₂O and heated at reflux under positive Ar pressure for 6 h while magnetic stirring was maintained. A solution of NH₄PF₆ (0.36 g, 2.2 mmol) in 10 mL of water was then filtered slowly into the stirring reaction mixture. The resulting precipitate was isolated by suction filtration and washed with water until the filtrate came through green. The solid was then washed well with anhydrous diethyl ether and air dried. The crude product was chromatographed on a 4 cm × 10 cm column of alumina packed in 2:1 CH₃CN/C₆H₅CH₃. The green solid was dissolved in a minimum of 2:1 CH₃CN/C₆H₅CH₃ and pipetted onto the column. Elution with 2:1 CH₃CN/C₆H₅CH₃ gave a green band of the dimer, which was preceded by an orange band and a blue band and followed by a dark band that remained at the top of the column. Gradual enrichment to 3:1 CH₃CN/C₆H₅CH₃ resulted in removal of the orange and blue bands which were discarded. Elution with 2% MeOH/CH₃CN was necessary to remove the green band, which was collected and taken to dryness on a rotary evaporator. The dimer was reprecipitated from CH₃CN/Et₂O to give a green solid in 49% yield. Anal. Calcd for [(C₁₀H₈N₂)₂Ru(C₈H₆N₄)Os(C₁₀H₈N₂)₂](PF₆)₄: C, 34.85; H, 2.32; N, 10.16. Found: C, 34.88; H, 2.52; N, 10.07.

[(bpy)₂Ru(py₂c)]PF₆. *cis*-(bpy)₂RuCl₂·2H₂O (0.244 g, 0.469 mmol) and 2-pyrazinecarboxylic acid (0.119 g, 0.959 mmol) were combined in 50 mL of 20% EtOH/H₂O containing ~2 mL of 2,6-lutidine. The mixture was heated to reflux under Ar while magnetic stirring was maintained. After 3 h, a solution of NH₄PF₆ (1.5 g, 9.3 mmol) in ~10 mL of H₂O was filtered dropwise into the hot, stirring reaction mixture. The mixture was allowed to cool to room temperature and

(9) Griffith, W. P. "The Chemistry of the Rarer Platinum Metals"; Interscience: New York, 1967.

(10) Calvert, J. M. Ph.D. Dissertation, The University of North Carolina, Chapel Hill, NC, 1981.

(11) Sullivan, B. P.; Salmon, D. J.; Meyer, T. J. *Inorg. Chem.* **1978**, *17*, 3334.

(12) (a) Kober, E. M. Ph.D. Dissertation, The University of North Carolina, Chapel Hill, NC, 1982. (b) Kober, E. M., unpublished results.

(13) Buckingham, D. A.; Dwyer, F. P.; Goodwin, H. A.; Sargeson, A. M. *Aust. J. Chem.* **1964**, *17*, 325.

(14) Sullivan, B. P.; Caspar, J. V.; Kober, E. M.; Meyer, T. J., manuscript in preparation.

(15) Dose, E. V.; Wilson, L. J. *Inorg. Chem.* **1978**, *17*, 2660.

(16) Rillema, D. P.; Mack, K. B. *Inorg. Chem.* **1982**, *21*, 3849.

then refrigerated for 24 h, resulting in crystallization of the orange-red complex. The microcrystalline solid was isolated by suction filtration, washed well with cold H₂O, and placed in a vacuum desiccator overnight. Yields ranged from 93% to 97%. Anal. Calcd for [(C₁₀H₈N₂)₂Ru(C₅H₃N₂O₂)]PF₆·2H₂O: C, 41.87; H, 2.95; N, 11.71. Found: C, 42.27; H, 3.22; N, 11.46.

[(bpy)₂ClRu(pyzc)Ru(bpy)₂](PF₆)₂. [(bpy)₂Ru(pyzc)]PF₆ (0.295 g, 0.433 mmol) and *cis*-(bpy)₂RuCl₂·2H₂O (0.337 g, 0.648 mmol) were combined in 20 mL of 50% EtOH/H₂O and heated to reflux under Ar while magnetic stirring was maintained. This and subsequent manipulations were carried out under reduced light. After 24 h, 15 mL of EtOH was added to the reaction mixture to remove solid that had deposited along the inside walls of the flask. This was followed by the addition of LiCl (0.304 g, 7.2 mmol). The reaction mixture was heated at reflux for an additional 2 h, after which a solution of excess NH₄PF₆ (1–2 g) in 10 mL of H₂O was filtered slowly into the stirring reaction mixture, yielding a purple precipitate. The solution volume was reduced by half on a rotary evaporator. The purple solid was isolated by suction filtration, washed well with H₂O followed by anhydrous diethyl ether, and air-dried for ~5 min. The crude dimer was purified by column chromatography. The purple solid was dissolved in a minimum amount of 1:1 CH₃CN/C₆H₅CH₃ and pipetted onto a 4 cm × 12 cm column of alumina packed in the same solvent mixture. Elution with 1:1 CH₃CN/C₆H₅CH₃ gave a purple band of the dimer, which was preceded by an orange band and followed by a dark blue that remained at the top of the column. Continued elution with 1:1 CH₃CN/C₆H₅CH₃ resulted in removal of the orange band, which was discarded. Gradual enrichment to 2:1 CH₃CN/C₆H₅CH₃ effected removal of the purple band, which was collected and taken to dryness on a rotary evaporator. The dimer was reprecipitated from CH₃CN/Et₂O to give a purple solid in 59% yield. Anal. Calcd for [(C₁₀H₈N₂)₂ClRu(C₅H₃N₂O₂)Ru(C₁₀H₈N₂)₂](PF₆)₂·H₂O: C, 41.78; H, 2.89; N, 10.83. Found: C, 41.53; H, 3.13; N, 10.70.

[(bpy)₂Os(pyzc)]PF₆. *cis*-(bpy)₂OsCl₂ (0.200 g, 0.349 mmol) and 2-pyrazinecarboxylic acid (0.217 g, 1.75 mmol) were combined in 50 mL of 20% EtOH/H₂O containing ~2 mL of 2,6-lutidine. The mixture was heated at reflux under Ar overnight while magnetic stirring was maintained. After this time, a solution of excess NH₄PF₆ (1–2 g) in ~10 mL of H₂O was filtered slowly into the stirring reaction mixture, yielding a dark green precipitate. The solution volume was reduced by half on a rotary evaporator, and then the solution was refrigerated for several h. The dark green solid was isolated by suction filtration, washed with 5 mL of cold H₂O, and placed in a vacuum desiccator overnight; yield 0.206 g (72%). Anal. Calcd for [(C₁₀H₈N₂)₂Os(C₅H₃N₂O₂)]PF₆·3H₂O: C, 36.41; H, 3.06; N, 10.19. Found: C, 36.11; H, 2.78; N, 9.57.

[(bpy)₂ClRu(pyzc)Os(bpy)₂](PF₆)₂. [(bpy)₂Os(pyzc)]PF₆ (0.241 g, 0.292 mmol) and *cis*-(bpy)₂RuCl₂·2H₂O (0.207 g, 0.398 mmol) were combined in 10 mL of 20% EtOH/H₂O and heated to reflux under Ar while magnetic stirring was maintained. This and subsequent manipulations were carried out under reduced light. After 24 h, 10 mL of EtOH was added to the reaction mixture to remove solid that had deposited along the inside walls of the flask. This was followed by the addition of LiCl (0.217 g, 5.1 mmol). The reaction mixture was heated at reflux for an additional 2 h, after which a solution of excess NH₄PF₆ (1–2 g) in ~10 mL of H₂O was filtered slowly into the stirring reaction mixture, yielding a purple precipitate. The solution volume was reduced by half on a rotary evaporator. The purple solid was isolated by suction filtration, washed well with H₂O followed by anhydrous diethyl ether, and air-dried for ~5 min. The crude dimer was purified by column chromatography. The purple solid was dissolved in a minimum amount of 1:1 CH₃CN/C₆H₅CH₃ and pipetted onto a 4 cm × 15 cm column of alumina packed in the same solvent mixture. Elution with 1:1 CH₃CN/C₆H₅CH₃ gave a purple band of the dimer, which was preceded by an orange band and a green band and followed by a dark band that remained at the top of the column. Continued elution with 1:1 CH₃CN/C₆H₅CH₃ resulted in removal of the orange and green bands, which were discarded. Gradual enrichment to 2:1 CH₃CN/C₆H₅CH₃ effected removal of the purple band, which was collected and taken to dryness on a rotary evaporator. The dimer was reprecipitated from CH₃CN/Et₂O to give a purple solid in 35% yield. Anal. Calcd for [(C₁₀H₈N₂)₂ClRu(C₅H₃N₂O₂)Os(C₁₀H₈N₂)₂](PF₆)₂·H₂O: C, 39.09; H, 2.70; N, 10.13. Found: C, 39.20; H, 3.12; N, 9.96.

Oxidation of Dimers. In order to obtain spectra of the IT bands, the mixed-valence dimers were prepared electrochemically by cou-

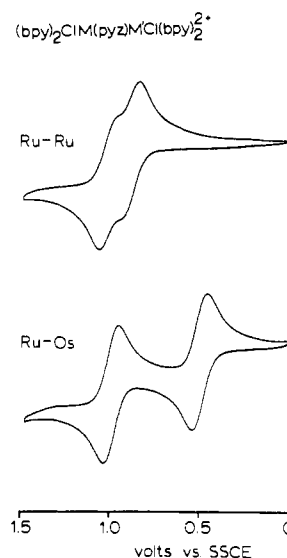


Figure 1. Cyclic voltammograms of the dimers [(bpy)₂ClRu(pyzc)RuCl(bpy)₂]²⁺ and [(bpy)₂ClRu(pyzc)OsCl(bpy)₂]²⁺ in 0.1 M TBAH/CH₃CN at 200 mV/s.

lometric oxidation of the analogous Ru^{II}-M^{II} (M = Ru, Os) dimers with a PAR Model 173 potentiostat. The oxidations were performed in three-compartment cells vs. SSCE, with a platinum screen employed as the working electrode. As with the cyclic and differential pulse measurements, Burdick & Jackson acetonitrile was employed as the electrochemical solvent and 0.1 M TBAH as the electrolyte. In the case of the Ru^{II}-Os^{II} dimers, where the separation between the two redox couples is substantial, the oxidations were performed at approximately 200 mV past (more positive than) the first E_{1/2}. The oxidations were considered complete after the current had fallen to 1% of the initial value. For the Ru^{II}-Ru^{II} dimers, the oxidations were followed with a PAR Model 179 digital coulometer. The oxidations were terminated after 1 equiv of electrons had been passed. After oxidation was complete, the oxidized solution was removed before significant mixing with the solutions in the other cell compartments could occur. The near-infrared spectra were obtained immediately following oxidation.

Results and Discussion

Preparation of Dimers. The scheme employed in the synthesis of the new dimers used in this work was relatively straightforward, especially in comparison to previously published preparations of chemically related dimers.² In general, a monomeric complex of the bridging ligand was allowed to react at reflux with 1.3 equiv of *cis*-(bpy)₂RuCl₂·2H₂O in ethanol/water for 12–48 h to give the resulting dimer in good yield (usually 40–60% based on monomer). Only for the bridging ligand 2,2'-bipyrimidine could the dimer be obtained in good yield by a one-pot reaction with 2 equiv of (bpy)₂RuCl₂·2H₂O.

The dimers were purified by column chromatography on alumina. In most cases, separation was achieved by elution with acetonitrile/toluene mixtures; however, for the highly charged (4+) bipyrimidine-bridged dimers, elution with 2% methanol in acetonitrile was required.

Electrochemistry. Cyclic voltammograms of the dimers [(bpy)₂ClRu^{II}(pyzc)Ru^{II}Cl(bpy)₂]²⁺ and [(bpy)₂ClRu^{II}(pyzc)Os^{II}Cl(bpy)₂]²⁺ are shown in Figure 1. Both dimers show two reversible anodic waves corresponding to consecutive one-electron oxidations at the two metal sites in each dimer. E_{1/2} values for the two pyrazine-bridged dimers were determined by differential pulse polarography and are given in Table II. A useful quantity for comparing different dimers is the difference potentials between the two couples, ΔE_{1/2} = E_{1/2}(M^{III}-M^{III}/M^{III}-M^{II}) - E_{1/2}(M^{III}-M^{II}/M^{II}-M^{II}), which gives a quantitative measure of the energetics for the com-

Table II. $E_{1/2}$ Data For the Dimeric Complexes in Acetonitrile^a

complex	$E_{1/2}(1),$ V^b	$E_{1/2}(2),$ V^b	$\Delta E_{1/2},$ V
$[(bpy)_2ClRu(pyzo)RuCl(bpy)_2]^{2+}$	0.89	1.02	0.13
$[(bpy)_2ClRu(pyzo)OsCl(bpy)_2]^{2+}$	0.51	1.01	0.50
$[(bpy)_2ClRu(4,4'-bpy)RuCl(bpy)_2]^{2+}$	0.80 ^c	0.85 ^c	0.05 ^c
$[(bpy)_2ClRu(4,4'-bpy)OsCl(bpy)_2]^{2+}$	0.41	0.83	0.42
$[(bpy)_2Ru(bpm)Ru(bpy)_2]^{4+}$	1.61	1.77 ^d	0.17
$[(bpy)_2Ru(bpm)Os(bpy)_2]^{4+}$	1.18	1.76 ^d	0.58
$[(bpy)_2ClRu(pyzo)Ru(bpy)_2]^{2+}$	0.93	1.14	0.21
$[(bpy)_2ClRu(pyzo)Os(bpy)_2]^{2+}$	0.62	1.06	0.44

^a Potentials were measured in 0.1 M TBAH/CH₃CN vs. SSCE at room temperature by differential pulse polarography. A Pt bead was used as the working electrode. ^b Error is ± 0.01 V. ^c Only one peak was observed in the differential pulse voltammograms. $\Delta E_{1/2}$ was estimated from the peak half-width with use of the technique of Richardson and Taube in: Richardson, D. E.; Taube, H. *Inorg. Chem.* 1981, 20, 1278. ^d These couples are irreversible by cyclic voltammetry in 0.1 M TBAH/CH₃CN vs. SSCE at a scan rate of 200 mV/s. Only the oxidation component was observed apparently because of rapid oxidation of the solvent or of an impurity in the solvent by the M^{III}-M^{III} dimer.

proportionation reaction ($K_{com} = \exp[-(\Delta G_{com}/RT)] = \exp(-\Delta E_{1/2}/RT)$):



In the symmetric Ru^{II}-Ru^{II} dimer, the redox couples are separated by 130 mV (i.e., $\Delta E_{1/2}(Ru-Ru) = 0.13$ V); however, $\Delta E_{1/2}(Ru-Os) = 0.50$ V for the structurally similar Ru^{II}-Os^{II} dimer. This is due to the lower oxidation potentials for Os complexes as compared to those for analogous Ru couples,¹⁷ as observed for all of the mixed-metal dimers investigated (see Table II).

For the symmetric dimers $[(bpy)_2ClRu(L)RuCl(bpy)_2]^{2+}$ (L = pyzo, 4,4'-bpy) and $[(bpy)_2Ru(bpm)Ru(bpy)_2]^{4+}$, the non-zero values for $\Delta E_{1/2}$ can be attributed to four factors: (1) electrostatics or ionization energies—since the second oxidation occurs adjacent to a greater positive charge than the first oxidation, it will occur at a higher potential; (2) solvation energies—the solvation energies will be different for the Ru^{II}-Ru^{II}, Ru^{II}-Ru^{III}, and Ru^{III}-Ru^{III} dimers; (3) delocalization or resonance—the unpaired electron is partially delocalized onto the Ru(III) site, shifting the second oxidation to potentials higher than one would expect with a totally localized electron; (4) statistical contributions—the Ru^{II}-Ru^{II} dimer can be oxidized to give either Ru^{II}-Ru^{III} or Ru^{III}-Ru^{II} and the Ru^{III}-Ru^{III} dimer reduced to give either Ru^{II}-Ru^{III} or Ru^{III}-Ru^{II}.²⁰

The ionization energy term leads to an increase in $\Delta E_{1/2}$ as the distance between metal sites is decreased while the solvation energy term varies in the opposite sense. The magnitude of the resonance energy term depends explicitly on the electronic properties of the metal ions and of the bridging ligand and, in any case, appears to be relatively small from the intensities of IT bands. From the above, the origin of the increase in $\Delta E_{1/2}$ as distance decreases must be in the ionization energy term.

The effects of ionization energy, solvation energies, and delocalization will also determine the magnitude of $\Delta E_{1/2}$ for the asymmetric dimers $[(bpy)_2ClRu(B)OsCl(bpy)_2]^{2+}$ (B =

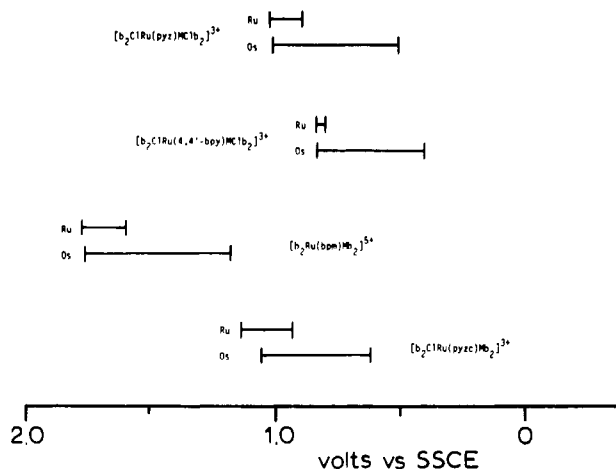


Figure 2. Schematic representation showing $\Delta E_{1/2}$ for the Ru-Ru and Ru-Os dimers.

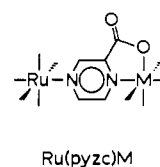


Figure 3. The dimeric structural unit based on the asymmetric bridging ligand 2-pyrazinecarboxylate.

pyzo, 4,4'-bpy), $[(bpy)_2Ru(bpm)Os(bpy)_2]^{4+}$, and $[(bpy)_2ClRu(pyzo)M(bpy)_2]^{2+}$ (M = Ru, Os). In the absence of significant electronic delocalization, the contributions to $\Delta E_{1/2}$ from electrostatic and solvation energy terms should be similar for analogous Ru-Ru and Ru-Os dimers, because they are closely related structurally. That this is the case experimentally can be seen by examining the data in Table II.

The point is illustrated in Figure 2, where $\Delta E_{1/2}$ values are represented schematically by horizontal lines, allowing a direct comparison to be made between Ru-Ru and Ru-Os dimers having the same bridging ligand. Recall that the first oxidation for the Ru-Os dimers occurs at a much lower potential than for the Ru-Ru dimers, because the oxidation is at Os^{II}. However, for each of the dimers involving symmetric bridging ligands (i.e., pyzo, 4,4'-bpy, and bpm) the second oxidation, which is at Ru^{II}, occurs at the same potential within experimental error in both the Ru-Ru and Ru-Os dimers. This observation suggests that the contribution to $\Delta E_{1/2}$ from the increased charge following the initial oxidation and from delocalization of the unpaired electron must be comparable for the analogous Ru-Ru and Ru-Os dimers. Such an observation is not surprising for these electronically weakly coupled dimers where the molecular dimensions of the Ru and Os units are expected to be nearly identical.

The situation is somewhat more complicated for the dimers $[(bpy)_2ClRu(pyzo)M(bpy)_2]^{2+}$ (M = Ru, Os) because the bridging ligand itself is unsymmetrical (note Table I). The metal-to-bridging-ligand bonding for the pyzo-bridged dimers is illustrated in Figure 3. The apparent reason for the decrease in the difference between $\Delta E_{1/2}$ values for the Ru-Ru and Ru-Os dimers is that there is a change in the initial site of oxidation induced by the electronic asymmetry of the bridging ligand. In the Ru-Ru dimer $[(bpy)_2ClRu(pyzo)Ru(bpy)_2]^{2+}$, the Ru-chloro side of the dimer is the first to be oxidized. However, for $[(bpy)_2ClRu(pyzo)Os(bpy)_2]^{2+}$, the Os-carboxylate side of the dimer is the first to be oxidized and a comparison like that for the symmetrical dimers is not possible. $E_{1/2}$ values for the Ru^{II/III} couples of related monomeric complexes are 0.95 V for $[(pyzo)Ru(bpy)_2]^+$, 0.56 V¹⁸ for $[(pyzo)Os(bpy)_2]^+$, and 0.88 V¹⁹ for $[(bpy)_2ClRu-$

(17) Taube, H. *Pure Appl. Chem.* 1979, 51, 901.

(18) $E_{1/2}$ for these complexes was determined by cyclic voltammetry in 0.1 M TBAH/CH₃CN at room temperature vs. SSCE.

(19) Callahan, R. W.; Brown, G. M.; Meyer, T. J. *Inorg. Chem.* 1975, 14, 1443.

(20) Callahan, R. W.; Keene, F. R.; Meyer, T. J.; Salmon, D. J. *J. Am. Chem. Soc.* 1977, 99, 1064.

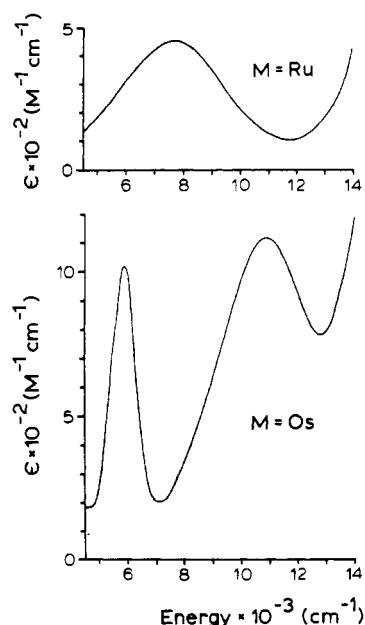


Figure 4. Near-infrared spectra of the mixed-valence dimers $[(\text{bpy})_2\text{ClRu}^{\text{II}}(\text{pyz})\text{M}^{\text{III}}\text{Cl}(\text{bpy})_2]^{3+}$ ($\text{M} = \text{Ru}, \text{Os}$) in acetonitrile.

$(\text{pyz})^+$. Our conclusion concerning the initial site of oxidation in the Ru dimer is based on a comparison between related monomer and dimer couples.

The first oxidation in $[(\text{bpy})_2\text{ClRu}(\text{pyzc})\text{Os}(\text{bpy})_2]^{2+}$ occurs 60 mV higher than that of the analogous Os monomer $[(\text{pyzc})\text{Os}(\text{bpy})_2]^+$. The first oxidation in $[(\text{bpy})_2\text{ClRu}(\text{pyzc})\text{Ru}(\text{bpy})_2]^{2+}$ occurs 20 mV lower than in the analogous Ru monomer $[(\text{pyzc})\text{Ru}(\text{bpy})_2]^+$ but 50 mV higher than in $[(\text{bpy})_2\text{ClRu}(\text{pyz})]^+$. A shift to positive potentials for dimers compared to monomers is a general feature for cationic Ru- and Os-bpy complexes because of the overall higher charge of the dimer, which makes oxidation of the dimer more difficult on electrostatic grounds. Clearly, the sense of the potential shift for $[(\text{bpy})_2\text{ClRu}(\text{pyzc})\text{Ru}(\text{bpy})_2]^{2+}$ compared to that for the two monomers is consistent with initial oxidation at the RuCl site.

Ultraviolet-Visible Spectra. Table III lists λ_{max} values and extinction coefficients (ϵ_{max}) for the new $\text{Ru}^{\text{II}}\text{-M}^{\text{III}}$ dimers and related monomers presented here. A typical spectrum consists of metal-to-ligand ($d\pi \rightarrow \pi^*$) charge-transfer bands in the visible region and ligand-localized $\pi \rightarrow \pi^*$ bands in the ultraviolet region.² The only point worth noting is that the Ru-Os spectra are generally more complex than the Ru-Ru spectra, and this is a consequence of greater spin-orbit coupling at the Os site.²²

Near-Infrared Spectra. The near-infrared (near-IR) spectra of the mixed-valence dimers $[(\text{bpy})_2\text{ClRu}^{\text{II}}(\text{pyz})\text{M}^{\text{III}}\text{Cl}(\text{bpy})_2]^{3+}$ ($\text{M} = \text{Ru}, \text{Os}$) are shown in Figure 4. The near-IR spectrum of the $\text{Ru}^{\text{II}}(\text{pyz})\text{Ru}^{\text{III}}$ dimer consists of a single, broad, featureless band, which has been assigned as an IT transition on the basis of its energy, its bandwidth, and the variation of the band energy with solvent.²⁰ The results of a more recent analysis²¹ suggest that the band is actually a manifold of three IT transitions which differ in the spin-orbit state reached at the optically prepared Ru^{III} site: $\text{Ru}^{\text{II}}\text{-Ru}^{\text{III}}$ $\xrightarrow{h\nu}$ $\text{Ru}^{\text{III}}(1E')\text{-Ru}^{\text{II}}$, $\text{Ru}^{\text{III}}(2E')\text{-Ru}^{\text{II}}$ or $\text{Ru}^{\text{III}}(3E')\text{-Ru}^{\text{II}}$. This is a consequence of the existence of three low-lying spin-orbit (SO) states associated with the d^5 core in lower than O_h symmetry. However, the band intensity is expected to be dominated by one of the three transitions,²¹ and we will treat

Table III. Ultraviolet-Visible Spectral Data for the New $\text{Ru}^{\text{II}}\text{-Ru}^{\text{II}}$ and $\text{Ru}^{\text{II}}\text{-Os}^{\text{II}}$ Dimers and Related Monomers in Acetonitrile

complex	λ_{max} , nm	ϵ_{max} , $\text{M}^{-1}\text{cm}^{-1}$	
$[(\text{bpy})_2\text{Os}^{\text{II}}(\text{bpm})]^{2+}$	635 (sh)		
	570 (sh)		
	455	1.3×10^4	
	435	1.3×10^4	
	370	1.2×10^4	
	350 (sh)		
	289	6.2×10^4	
	255 (sh)		
	244	3.5×10^4	
	468	1.2×10^4	
	$[(\text{pyzc})\text{Ru}^{\text{II}}(\text{bpy})_2]^+$	445 (sh)	
		400 (sh)	
332		6.6×10^3	
292		5.2×10^4	
270 (sh)			
256		1.9×10^4	
$[(\text{pyzc})\text{Os}^{\text{II}}(\text{bpy})_2]^+$		715 (sh)	
		625	4.3×10^3
		555 (sh)	
		495 (sh)	
		480	1.4×10^4
		418	1.3×10^4
	400 (sh)		
	342	7.5×10^3	
	293	5.8×10^4	
	270 (sh)		
	256	2.2×10^4	
	$[(\text{bpy})_2\text{ClRu}^{\text{II}}(4,4'\text{-bpy})\text{Os}^{\text{II}}\text{Cl}(\text{bpy})_2]^{2+}$	665 (sh)	
540 (sh)			
500		2.8×10^4	
465 (sh)			
428		2.2×10^4	
410 (sh)			
362		1.5×10^4	
295		9.8×10^4	
260 (sh)			
$[(\text{bpy})_2\text{Ru}^{\text{II}}(\text{bpm})\text{Os}^{\text{II}}(\text{bpy})_2]^{4+}$		617	1.0×10^4
		560 (sh)	
		515 (sh)	
	415	3.1×10^4	
	395 (sh)		
	282	1.1×10^5	
	250 (sh)		
	244	5.5×10^4	
	$[(\text{bpy})_2\text{ClRu}^{\text{II}}(\text{pyzc})\text{Ru}^{\text{II}}(\text{bpy})_2]^{2+}$	600 (sh)	
		534	2.4×10^4
		478	1.9×10^4
		338	1.1×10^4
292		6.3×10^4	
255 (sh)			
$[(\text{bpy})_2\text{ClRu}^{\text{II}}(\text{pyzc})\text{Os}^{\text{II}}(\text{bpy})_2]^{2+}$		553	2.5×10^4
		481	2.0×10^4
		400 (sh)	
		343	1.3×10^4
		292	8.6×10^4
		280 (sh)	

the manifold as a single band.

The near-IR spectrum of $[(\text{bpy})_2\text{ClRu}^{\text{II}}(\text{pyz})\text{Os}^{\text{III}}\text{Cl}(\text{bpy})_2]^{3+}$ is more congested, consisting of two bands: a broad band at 10900 cm^{-1} and a much narrower band at 5900 cm^{-1} . The existence of the additional narrow band in the $\text{Ru}^{\text{II}}\text{-Os}^{\text{III}}$ spectrum is due to a transition between different spin-orbit states localized at Os(III).^{12,22}

The relative energy spacings between the ground state ($1E'$) and the two spin-orbit excited states ($2E'$, $3E'$) are determined by the magnitude of the SO coupling constant and the nature of the surrounding ligands.²² In the case of Os(III), the SO

(21) Kober, E. M.; Goldsby, K. A.; Narayana, D. N. S.; Meyer, T. J. *J. Am. Chem. Soc.* **1983**, *105*, 4303.

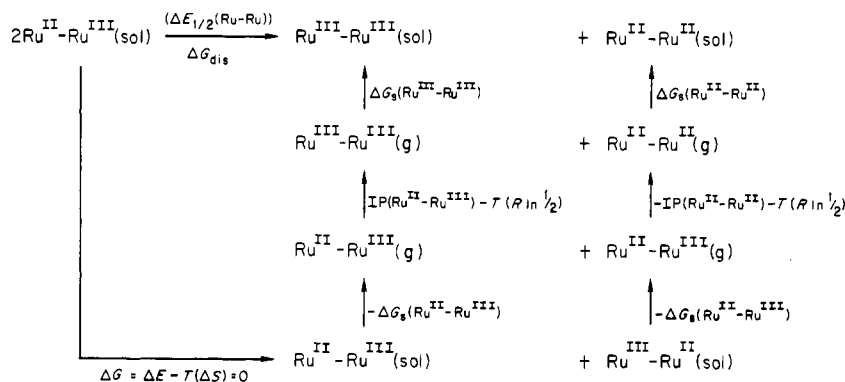
(22) (a) Goodman, B. A.; Raynor, J. B. *Adv. Inorg. Radiochem.* **1970**, *13*, 192. (b) Kober, E. M.; Meyer, T. J. *Inorg. Chem.* **1982**, *21*, 3967.

Table IV. ΔE_{op} and $\Delta(\Delta E_{1/2})$ for the Mixed-Valence Dimers in Acetonitrile

complex	M	$10^{-3} E_{op}$, cm ⁻¹	$10^{-3} \Delta E_{op}$, cm ⁻¹	$10^{-3} \Delta E_{1/2}$, cm ⁻¹	$10^{-3} \Delta(\Delta E_{1/2})$, cm ⁻¹
[(bpy) ₂ ClRu(pyzo)MCl(bpy) ₂] ³⁺	Ru	7.69 ± 0.05 ^a	3.17 ± 0.07	1.05 ± 0.11	2.98 ± 0.15
	Os	10.86 ± 0.05		4.03 ± 0.11	
[(bpy) ₂ ClRu(4,4'-bpy)MCl(bpy) ₂] ³⁺	Ru	10.15 ± 0.05 ^a	3.1 ± 0.2	0.39 ± 0.04	3.00 ± 0.12
	Os	13.3 ± 0.2		3.39 ± 0.11	
[(bpy) ₂ Ru(bpm)M(bpy) ₂] ³⁺	Ru	5.0 ± 0.3	3.1 ± 0.3	1.37 ± 0.11	3.31 ± 0.15
	Os	8.08 ± 0.05		4.68 ± 0.11	
[(bpy) ₂ ClRu(pyzo)M(bpy) ₂] ³⁺	Ru	8.77 ± 0.05	1.70 ± 0.07	1.59 ± 0.11	1.86 ± 0.15
	Os	10.47 ± 0.05		3.55 ± 0.11	

^a Reference 2.

Scheme I



coupling constant is sufficiently large that the transitions are observable in the near-IR region. For the monomer [(bpy)₂ClO^{III}pyz]²⁺, two bands are observed at energies 4240 and 6330 cm⁻¹, corresponding to the 1E' → 2E' and 1E' → 3E' transitions, respectively.^{12a}

Returning to the Ru^{II}(pyz)Os^{III} dimer, we note that the narrow band at 5900 cm⁻¹ corresponds to the 1E' → 3E' transition localized on the Os^{III} site. The dimer exhibits an additional transition at 4200 cm⁻¹ not shown in Figure 4, which corresponds to the 1E' → 2E' transition.^{12b} Note the similarity in energy for the 1E' → 3E' transitions between the monomer [(bpy)₂ClO^{III}(pyz)]²⁺ and the Ru^{II}(pyz)Os^{III} dimer.

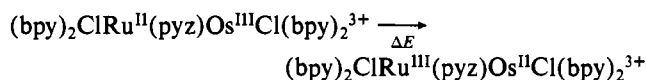
With the lower energy band in the bottom part of Figure 4 assigned as the 1E' → 3E' transition localized at the Os^{III} site, attention can be turned to the broader band at 10 900 cm⁻¹. This band has been assigned as the IT transition shown in eq 1, based on its bandwidth, intensity, and its variation in energy with solvent.^{6,12b} In fact, the bandwidth and solvent dependences for the Ru^{II}(pyz)Os^{III} and Ru^{II}(pyz)Ru^{III} dimers are virtually the same. The principal difference between the two bands is that λ_{max} for the Ru^{II}(pyz)Os^{III} IT band occurs 3200 cm⁻¹ higher in energy than λ_{max} for the Ru^{II}(pyz)Ru^{III} dimer.

The IT band maxima (E_{op}) for all of the mixed-valence dimers are listed in Table IV. In every case, E_{op} for the Ru^{II}-Os^{III} dimer is greater than E_{op} for the analogous Ru^{II}-Ru^{III} dimer. This is the qualitative prediction of eq 2a, which states that, for mixed-valence systems having similar values for χ_i and χ_o , E_{op} should increase with increasing ΔE . In order to establish the validity of eq 2a with respect to the dimers in Table IV, it is necessary to obtain an estimate for ΔE , and such an estimate is available from the electrochemical data.

Relationship between E_{op} and $\Delta E_{1/2}$. The $\Delta E_{1/2}$ values for all the dimers in Table II are relisted in Table IV in units of cm⁻¹ along with the IT band energies so that the two quantities can be used interchangeably.

The goal of this section is to obtain estimates for ΔE from the electrochemical data. Note that ΔE is the internal energy

difference between the different oxidation-state isomers connected by the optical transition, e.g.

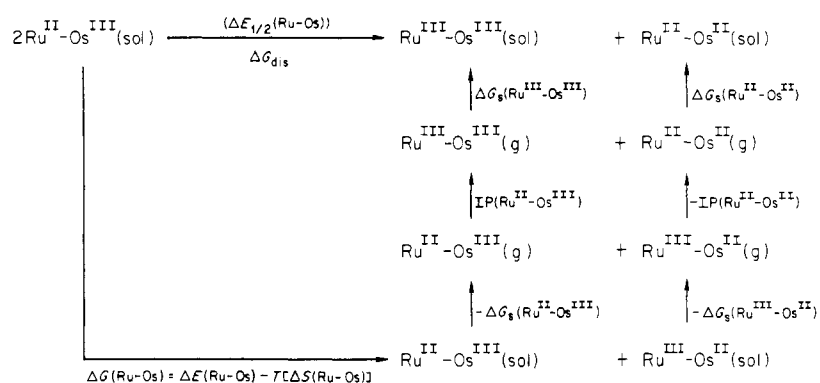


For a symmetric mixed-valence dimer such as [(bpy)₂ClRu^{II}(pyz)Ru^{III}Cl(bpy)₂]³⁺, $\Delta E = 0$, since there is no difference between the oxidation-state isomers Ru^{II}-Ru^{III} and Ru^{III}-Ru^{II}. However, the difference in redox potentials between Ru^{III/II} couples for the first, Ru^{II}-Ru^{II} → Ru^{III}-Ru^{III} + e⁻, and second, Ru^{II}-Ru^{III} → Ru^{III}-Ru^{III} + e⁻, oxidations is non-zero because of the combined effects of ionization energy, delocalization, and solvation energies as noted earlier. The contributions from the various terms are illustrated in the thermodynamic cycle shown in Scheme I for a Ru^{II}-Ru^{III} dimer. The terms (sol) and (g) that appear in the cycle refer to the solution and gaseous states, respectively. As written, the $\Delta E_{1/2}$ values in Table II are the free energies of disproportionation of the mixed-valence dimer into the Ru^{II}-Ru^{II} and Ru^{III}-Ru^{III} dimers, $\Delta E_{1/2} = \Delta G_{dis} (V) = -\Delta G_{com} (V)$. The value of the cycle is that it relates $\Delta E_{1/2}$ from the electrochemical measurements to the quantity needed for the spectral correlation, ΔE for the reaction Ru^{II}-Ru^{III} → Ru^{III}-Ru^{II}. From the cycle, $\Delta E_{1/2}(Ru-Ru)$ can be expressed in terms of (1) the ionization energy (IP) of the mixed-valence dimer, IP(Ru^{II}-Ru^{III}), (2) the ionization energy of the reduced dimer, IP(Ru^{II}-Ru^{II}), (3) a series of free energy of solvation terms, ΔG_s , and (4) a statistical factor, $-T(\Delta S) = -T(R \ln 1/2)$ (note eq 5). In eq 5, contributions to $\Delta E_{1/2}$ from electrostatic and delocalization are included in the IP terms.

$$\Delta E_{1/2}(Ru-Ru) = [IP(Ru^{II}-Ru^{III}) - IP(Ru^{II}-Ru^{II})] + [\Delta G_s(Ru^{III}-Ru^{III}) + \Delta G_s(Ru^{II}-Ru^{II}) - 2(\Delta G_s(Ru^{II}-Ru^{III}))] + RT \ln 4 \quad (5)$$

A related cycle for a Ru^{II}-Os^{III} dimer is shown in Scheme II. Note that in this cycle the term IP(Ru^{II}-Os^{II}) refers to an excited-state ionization process. In the ionization, the electron is lost from the Ru^{II} rather than from Os^{II}, which is

Scheme II



avored thermodynamically. For the Ru–Os cycle, eq 6 is obtained. Given the essentially identical molecular structures

$$\begin{aligned}
 \Delta E_{1/2}(\text{Ru}-\text{Os}) &= \Delta E(\text{Ru}-\text{Os}) - T[\Delta S(\text{Ru}-\text{Os})] + \\
 &[\text{IP}(\text{Ru}^{\text{II}}-\text{Os}^{\text{III}}) - \text{IP}(\text{Ru}^{\text{II}}-\text{Os}^{\text{II}})] + [\Delta G_{\text{s}}(\text{Ru}^{\text{III}}-\text{Os}^{\text{III}}) + \\
 &\Delta G_{\text{s}}(\text{Ru}^{\text{II}}-\text{Os}^{\text{II}}) - \Delta G_{\text{s}}(\text{Ru}^{\text{II}}-\text{Os}^{\text{III}}) - \Delta G_{\text{s}}(\text{Ru}^{\text{III}}-\text{Os}^{\text{II}})] \quad (6)
 \end{aligned}$$

expected for related Ru–Ru and Ru–Os dimers, the free energies of solvation should be roughly the same for the two dimers; i.e., $\Delta G_{\text{s}}(\text{Ru}^{\text{II}}-\text{Ru}^{\text{II}}) \approx \Delta G_{\text{s}}(\text{Ru}^{\text{II}}-\text{Os}^{\text{II}})$, $\Delta G_{\text{s}}(\text{Ru}^{\text{II}}-\text{Ru}^{\text{III}}) \approx \Delta G_{\text{s}}(\text{Ru}^{\text{II}}-\text{Os}^{\text{III}})$, etc. Furthermore, given the weak electronic coupling in these dimers (note a later section), variations in the IP terms are expected to be dominated by electrostatic interactions which should be the same whether a Ru or Os ion is adjacent to Ru(II). Consequently, for structurally analogous dimers, i.e., $\text{IP}(\text{Ru}^{\text{II}}-\text{Ru}^{\text{III}}) \approx \text{IP}(\text{Ru}^{\text{II}}-\text{Os}^{\text{III}})$ and $\text{IP}(\text{Ru}^{\text{II}}-\text{Ru}^{\text{II}}) \approx \text{IP}(\text{Ru}^{\text{II}}-\text{Os}^{\text{II}})$. Assuming these approximations to be valid, subtracting eq 5 from eq 6 gives

$$\begin{aligned}
 \Delta E_{1/2}(\text{Ru}-\text{Os}) - \Delta E_{1/2}(\text{Ru}-\text{Ru}) &= \Delta(\Delta E_{1/2}) = \\
 &\Delta E(\text{Ru}-\text{Os}) - T[\Delta S(\text{Ru}-\text{Os})] - 2RT \ln 2 \quad (7)
 \end{aligned}$$

There is no change in electronic degeneracy between the oxidation-state isomers to contribute to ΔS . Although significant contributions to $\Delta S(\text{Ru}-\text{Os})$ could come from changes in solvation, since the coordination environments are identical on either side of the dimer, $\Delta S(\text{Ru}-\text{Os})$ should be negligible. The statistical factor is also small ($2RT \ln 2 = 36 \text{ mV}$) and can be neglected, yielding

$$\Delta(\Delta E_{1/2}) \approx \Delta E(\text{Ru}-\text{Os}) \quad (8)$$

Substituting $\Delta E(\text{Ru}-\text{Ru}) = 0$ and eq 8 into eq 2a gives eq 9 and 10. According to eq 11, for analogous $\text{Ru}^{\text{II}}-\text{Ru}^{\text{III}}$ and

$$E_{\text{op}}(\text{Ru}^{\text{II}}-\text{Ru}^{\text{III}}) = \chi_i + \chi_o \quad (9)$$

$$E_{\text{op}}(\text{Ru}^{\text{II}}-\text{Os}^{\text{III}}) = \chi_i + \chi_o + \Delta(\Delta E_{1/2}) \quad (10)$$

$$E_{\text{op}}(\text{Ru}^{\text{II}}-\text{Os}^{\text{III}}) - E_{\text{op}}(\text{Ru}^{\text{II}}-\text{Ru}^{\text{III}}) = \Delta E_{\text{op}} = \Delta(\Delta E_{1/2}) \quad (11)$$

$\text{Ru}^{\text{II}}-\text{Os}^{\text{III}}$ dimers containing symmetrical bridging ligands, the IT band for the $\text{Ru}^{\text{II}}-\text{Os}^{\text{III}}$ dimer will be higher in energy by an amount equal to $\Delta(\Delta E_{1/2})$. Inspection of Table III shows that $\Delta E_{\text{op}} = \Delta(\Delta E_{1/2})$ within experimental error for each of the symmetrically bridged dimers. This agreement between spectral and electrochemical measurements represents an important validation of eq 2a.

For the dimers with the unsymmetrical bridging ligand $[(\text{bpy})_2\text{ClRu}(\text{pyzc})\text{M}(\text{bpy})_2]^{3+}$ ($\text{M} = \text{Ru}, \text{Os}$), it is not possible to estimate ΔE from electrochemical measurements alone, since $\Delta E \neq 0$ for the Ru–Ru dimer. However, an expression for ΔE_{op} in terms of redox potentials can still be derived. Employing a thermochemical cycle similar to the one shown

for the symmetrically bridged Ru–Os dimer leads to expressions relating ΔE and $\Delta E_{1/2}$ for the pyzc-bridged dimers as shown in eq 12 and 13. Applying the same procedures and

$$\begin{aligned}
 \Delta E_{1/2}(\text{Ru}(\text{pyzc})\text{Ru}) &= \Delta E(\text{Ru}^{\text{III}}(\text{pyzc})\text{Ru}^{\text{II}}) - \\
 &T[\Delta S(\text{Ru}^{\text{III}}(\text{pyzc})\text{Ru}^{\text{II}})] + \text{IP}(\text{Ru}^{\text{III}}(\text{pyzc})\text{Ru}^{\text{II}}) - \\
 &\text{IP}(\text{Ru}^{\text{II}}(\text{pyzc})\text{Ru}^{\text{II}}) + [\Delta G_{\text{s}}(\text{Ru}^{\text{III}}(\text{pyzc})\text{Ru}^{\text{III}}) + \\
 &\Delta G_{\text{s}}(\text{Ru}^{\text{II}}(\text{pyzc})\text{Ru}^{\text{II}}) - \Delta G_{\text{s}}(\text{Ru}^{\text{III}}(\text{pyzc})\text{Ru}^{\text{II}}) - \\
 &\Delta G_{\text{s}}(\text{Ru}^{\text{II}}(\text{pyzc})\text{Ru}^{\text{III}})] \quad (12)
 \end{aligned}$$

$$\begin{aligned}
 \Delta E_{1/2}(\text{Ru}(\text{pyzc})\text{Os}) &= \Delta E(\text{Ru}^{\text{II}}(\text{pyzc})\text{Os}^{\text{III}}) - \\
 &T[\Delta S(\text{Ru}^{\text{II}}(\text{pyzc})\text{Os}^{\text{III}})] + \text{IP}(\text{Ru}^{\text{II}}(\text{pyzc})\text{Os}^{\text{III}}) - \\
 &\text{IP}(\text{Ru}^{\text{II}}(\text{pyzc})\text{Os}^{\text{II}}) + [\Delta G_{\text{s}}(\text{Ru}^{\text{III}}(\text{pyzc})\text{Os}^{\text{III}}) + \\
 &\Delta G_{\text{s}}(\text{Ru}^{\text{II}}(\text{pyzc})\text{Os}^{\text{II}}) - \Delta G_{\text{s}}(\text{Ru}^{\text{II}}(\text{pyzc})\text{Os}^{\text{III}}) - \\
 &\Delta G_{\text{s}}(\text{Ru}^{\text{III}}(\text{pyzc})\text{Os}^{\text{II}})] \quad (13)
 \end{aligned}$$

approximations as before gives eq 14, which is the same result

$$E_{\text{op}}(\text{Ru}^{\text{II}}(\text{pyzc})\text{Os}^{\text{III}}) - E_{\text{op}}(\text{Ru}^{\text{III}}(\text{pyzc})\text{Ru}^{\text{II}}) = \Delta E_{\text{op}} = \Delta(\Delta E_{1/2}) \quad (14)$$

obtained for the mixed-valence dimers containing a symmetrical bridging ligand (eq 11). As shown by the data in Table IV, ΔE_{op} and $\Delta(\Delta E_{1/2})$ are equal within experimental error for the pyzc-bridged dimers, once again suggesting that E_{op} varies with ΔE as predicted by eq 2a.

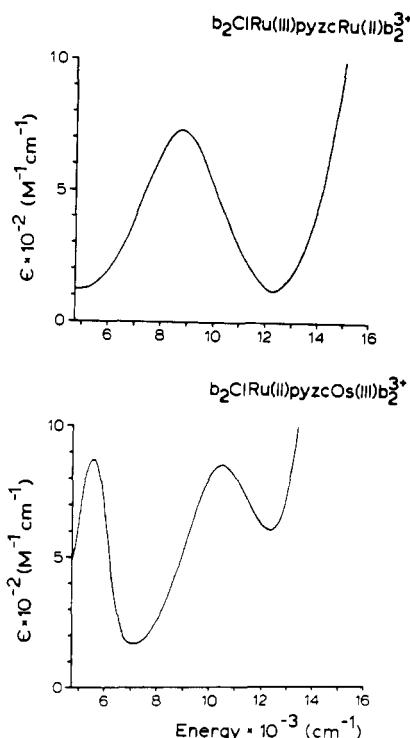
A few comments relating our conclusions to the existence of multiple spin-orbit states at Ru(III) are in order. As discussed above, the effect of SO coupling is to create three electronic states at the M(III) site, any one of which can be formed by intervalence transfer,²¹ and the IT manifold may include contributions from all transitions. Even so, the treatment based on eq 5–14 remains valid. If contributions from higher energy SO states appear in the intervalence-transfer band, they simply introduce an additional term into the thermodynamic cycles for the analogous Ru–Ru and Ru–Os dimers. Since the geometries and coordination spheres of the optically produced Ru(III) site are essentially the same irregardless of whether a prior Os site is adjacent,²³ the splitting between SO states and the d orbital which dominates in the IT process should also be the same. The net result is that the effects of contributions from multiple SO states will cancel for the two dimers.

The Vibrational Reorganization Energy, χ . In the previous section, the correlation between ΔE_{op} and $\Delta(\Delta E_{1/2})$ in eq 11 and 14 depended upon the assumption that χ is roughly the same for structurally analogous dimers of Ru and Os. If χ is comparable for the two types of dimers, the fact should be reflected in the band shapes of the IT bands. In Table V are

(23) Technically this is only true for the symmetrically bridged dimers; however, for the pyzc-bridged dimers, the coordination environments are very similar as shown by the similarities in redox potentials for the monomeric components.

Table V. Experimental and Theoretical^a Bandwidths at Half-Height for the Mixed-Valence Dimers in Acetonitrile

complex	$10^{-3} \times \Delta\bar{\nu}_{1/2, \text{exptl}}, \text{cm}^{-1}$	$10^{-3} \times \Delta\bar{\nu}_{1/2, \text{theor}}, \text{cm}^{-1}$
$[(\text{bpy})_2\text{ClRu}(\text{pyz})\text{RuCl}(\text{bpy})_2]^{3+}$	4.5 ^b	4.2
$[(\text{bpy})_2\text{ClRu}(\text{pyz})\text{OsCl}(\text{bpy})_2]^{3+}$	4.3	4.1
$[(\text{bpy})_2\text{ClRu}(4,4'\text{-bpy})\text{RuCl}(\text{bpy})_2]^{3+}$	5.2 ^b	4.8
$[(\text{bpy})_2\text{ClRu}(4,4'\text{-bpy})\text{OsCl}(\text{bpy})_2]^{3+}$	4.9	4.9
$[(\text{bpy})_2\text{Ru}(\text{bpm})\text{Ru}(\text{bpy})_2]^{5+}$	<i>c</i>	3.4
$[(\text{bpy})_2\text{Ru}(\text{bpm})\text{Os}(\text{bpy})_2]^{5+}$	4.4	3.4
$[(\text{bpy})_2\text{ClRu}(\text{pyzc})\text{Ru}(\text{bpy})_2]^{3+}$	3.7	4.3
$[(\text{bpy})_2\text{ClRu}(\text{pyzc})\text{Os}(\text{bpy})_2]^{3+}$	3.6	4.4

^a Calculated from eq 3 assuming room temperature as 25 °C.^b Reference 2. ^c The $\text{Ru}^{\text{II}}(\text{bpm})\text{Ru}^{\text{III}}$ dimer was not sufficiently stable for a meaningful bandwidth to be obtained.**Figure 5.** Near-infrared spectra of the mixed-valence dimers $[(\text{bpy})_2\text{ClRu}^{\text{III}}(\text{pyzc})\text{Ru}^{\text{II}}(\text{bpy})_2]^{3+}$ and $[(\text{bpy})_2\text{ClRu}^{\text{II}}(\text{pyzc})\text{Os}^{\text{III}}(\text{bpy})_2]^{3+}$ in acetonitrile. In the figure, b is bpy.

listed the experimental and theoretical (calculated from eq 3) bandwidths at half-height— $\Delta\bar{\nu}_{1/2, \text{exptl}}$ and $\Delta\bar{\nu}_{1/2, \text{theor}}$, respectively—for the $\text{Ru}^{\text{II}}\text{—Ru}^{\text{III}}$ and $\text{Ru}^{\text{II}}\text{—Os}^{\text{III}}$ dimers.

When experimental values for $\Delta\bar{\nu}_{1/2}$ ²⁴ are compared with values calculated by using the classical result in eq 3, it is generally observed that $\Delta\bar{\nu}_{1/2, \text{exptl}} > \Delta\bar{\nu}_{1/2, \text{theor}}$. For the dimers

(24) $\Delta\bar{\nu}_{1/2, \text{exptl}}$ was calculated by taking the difference in the energies of the IT band, for which $A(\bar{\nu}) = A_{\text{max}}/2$, where $A(\bar{\nu})$ is the absorbance at $\bar{\nu}$. For the high-energy IT bands (e.g., all of the $\text{Ru}^{\text{II}}\text{—Os}^{\text{III}}$ IT bands) where the high-energy side of the band is obscured by intense $\text{M}^{\text{II}} \rightarrow \text{bpy}$ charge-transfer bands, $\Delta\bar{\nu}_{1/2, \text{exptl}}$ was obtained by doubling the half-bandwidth on the low-energy side. It should be pointed out that eq 3 was derived for the case where wavelength-intensity corrections have been made so that the bandwidth is defined as the value of $\Delta\bar{\nu}$ for which

$$\frac{[A(\bar{\nu})]_{\bar{\nu}_{\text{max}}}}{A_{\text{max}}} = \frac{1}{2}$$

(note ref 1b). For bands in the near-IR spectral region, the bandwidths as determined by using the equation above are at most somewhat larger than the values obtained by using $A(\bar{\nu}) = A_{\text{max}}/2$. Furthermore, the high-energy side of the $\text{Ru}^{\text{II}}\text{—Os}^{\text{III}}$ IT bands are too obscured to use the wavelength-intensity correcting criterion. Therefore, in order that comparisons could be made between the $\text{Ru}^{\text{II}}\text{—Ru}^{\text{III}}$ and $\text{Ru}^{\text{II}}\text{—Os}^{\text{III}}$ bandwidths, the simpler $A(\bar{\nu}) = A_{\text{max}}/2$ criterion was used.

Table VI. Extinction Coefficients, Internuclear Separation Distances, and α^2 for the Mixed-Valence Dimers

complex	$\epsilon_{\text{max}}, \text{M}^{-1} \text{cm}^{-1}$	<i>d</i> , Å ^b	α^2 ^c
$[(\text{bpy})_2\text{ClRu}(\text{pyz})\text{RuCl}(\text{bpy})_2]^{3+}$	455 ^b	6.9	2.6×10^{-3}
$[(\text{bpy})_2\text{ClRu}(\text{pyz})\text{OsCl}(\text{bpy})_2]^{3+}$	1120	6.9	4.6×10^{-3}
$[(\text{bpy})_2\text{ClRu}(4,4'\text{-bpy})\text{RuCl}(\text{bpy})_2]^{3+}$	180 ^b	11.1	3.6×10^{-4}
$[(\text{bpy})_2\text{ClRu}(4,4'\text{-bpy})\text{OsCl}(\text{bpy})_2]^{3+}$	370	11.1	5.4×10^{-4}
$[(\text{bpy})_2\text{Ru}(\text{bpm})\text{Ru}(\text{bpy})_2]^{5+}$	<i>d</i>	5.6	—
$[(\text{bpy})_2\text{Ru}(\text{bpm})\text{Os}(\text{bpy})_2]^{5+}$	330	5.6	2.4×10^{-3}
$[(\text{bpy})_2\text{ClRu}(\text{pyzc})\text{Ru}(\text{bpy})_2]^{3+}$	730	6.9	2.7×10^{-3}
$[(\text{bpy})_2\text{ClRu}(\text{pyzc})\text{Os}(\text{bpy})_2]^{3+}$	850	6.9	2.4×10^{-3}

^a In CH_3CN . ^b Reference 2. ^c Calculated by using eq 15.^d The $\text{Ru}^{\text{II}}(\text{bpm})\text{Ru}^{\text{III}}$ complex was not sufficiently stable for a meaningful bandwidth to be obtained.

of interest here, broader bands are expected on two grounds: (1) as mentioned earlier, the IT band is actually a manifold of three IT transitions involving different SO states;²¹ (2) eq 3 is derived in the classical limit,¹ $\hbar\omega \ll kT$. For the dimers of interest here, recent X-ray crystallographic studies on related monomers show that nonnegligible contributions are expected from Ru—Cl and to a lesser extent Ru—N vibrational modes with vibrational frequencies in the range 200–400 cm^{-1} , while $k_B T = 200 \text{ cm}^{-1}$ at room temperature.²⁵ Inclusion of such modes would also result in a broadening of the absorption envelopes. In Table V $\Delta\bar{\nu}_{1/2, \text{exptl}} > \Delta\bar{\nu}_{1/2, \text{theor}}$ for all the mixed-valence dimers except $\text{Ru}^{\text{III}}(\text{pyzc})\text{Ru}^{\text{II}}$ and $\text{Ru}^{\text{II}}(\text{pyzc})\text{Os}^{\text{III}}$; however, even for these dimers, the IT bands are much broader than the accompanying SO coupling transitions (see Figure 5).

The most important comparison of bandwidths to be made in Table V is that of $\Delta\bar{\nu}_{1/2, \text{exptl}}$ between structurally analogous $\text{Ru}^{\text{II}}\text{—Ru}^{\text{III}}$ and $\text{Ru}^{\text{II}}\text{—Os}^{\text{III}}$ dimers. For the pyz-, 4,4'-bpy-, and pyzc-bridged dimers, $\Delta\bar{\nu}_{1/2, \text{exptl}}(\text{Ru}^{\text{II}}\text{—Ru}^{\text{III}}) \approx \Delta\bar{\nu}_{1/2, \text{exptl}}(\text{Ru}^{\text{II}}\text{—Os}^{\text{III}})$. In fact, $\Delta\bar{\nu}_{1/2, \text{exptl}}(\text{Ru}^{\text{II}}\text{—Os}^{\text{III}})$ is always slightly less than $\Delta\bar{\nu}_{1/2, \text{exptl}}(\text{Ru}^{\text{II}}\text{—Ru}^{\text{III}})$, and this may be attributed to the location of the IT band of the $\text{Ru}^{\text{II}}\text{—Os}^{\text{III}}$ dimers on the tail of intense $\text{Ru}^{\text{II}} \rightarrow$ ligand charge-transfer transitions (note Figures 4 and 5), which tends to compress the bandwidth of the IT band. Unfortunately, the mixed-valence form of the $\text{Ru}(\text{bpm})\text{Ru}$ dimer was not sufficiently stable for a meaningful bandwidth to be obtained. The agreement in bandwidths for the analogous $\text{Ru}^{\text{II}}\text{—Ru}^{\text{III}}$ and $\text{Ru}^{\text{II}}\text{—Os}^{\text{III}}$ dimers suggests that χ must also be similar, which was an important assumption in the previous section.

Electronic Delocalization. As shown by Hush, an estimate for the extent of delocalization α^2 can be made from IT band intensities with use of eq 15, where ϵ_{max} is the extinction coefficient of the IT band in $\text{M}^{-1} \text{cm}^{-1}$ and *d*, the distance between redox sites, is in Å.¹ In Table VI, ϵ_{max} and α^2 are

$$\alpha^2 = \frac{(4.2 \times 10^{-4})\epsilon_{\text{max}}\Delta\bar{\nu}_{1/2}}{d^2 E_{\text{op}}} \quad (15)$$

reported for the various $\text{Ru}^{\text{II}}\text{—Ru}^{\text{III}}$ and $\text{Ru}^{\text{II}}\text{—Os}^{\text{III}}$ dimers. Note that the small values for α^2 support the suggestion that electronic coupling between sites is weak.

For the three pairs of dimers where comparison is possible, the $\text{Ru}^{\text{II}}\text{—Os}^{\text{III}}$ IT band has the greater extinction coefficient. However, E_{op} is also greater for the $\text{Ru}^{\text{II}}\text{—Os}^{\text{III}}$ IT band because of the redox asymmetry and the net effect (note eq 15) is that α^2 is comparable for the $\text{Ru}^{\text{II}}\text{—Ru}^{\text{III}}$ and $\text{Ru}^{\text{II}}\text{—Os}^{\text{III}}$ dimers. The fact that α^2 is approximately the same for the $\text{Ru}^{\text{II}}\text{—Ru}^{\text{III}}$ and $\text{Ru}^{\text{II}}\text{—Os}^{\text{III}}$ dimers, even though the d-orbital extension is

(25) Eggleston, D. S.; Goldsby, K. A.; Hodgson, D. J.; Meyer, T. J., manuscript in preparation.

greater for Os than for Ru ($5d_{Os}$ vs. $4d_{Ru}$), indicates that the coupling between sites is dominated by Ru^{II} -bridging-ligand mixing, as assumed in the treatment of Richardson and Taube.²⁶ Therefore, the effects of delocalization for the structurally analogous Ru^{II} - Ru^{III} and Ru^{II} - Os^{III} dimers should be roughly the same. A last point is that α^2 is small, supporting the assumption that electrostatics and solvation energies provide the dominant factors in determining the magnitude of $\Delta(\Delta E_{1/2})$.

Acknowledgment is made to the Army Research Office—Durham, under Grant No. DAAG29-82-K-0111, for support of this research.

(26) Richardson, D. E.; Taube, H. *J. Am. Chem. Soc.* **1983**, *105*, 40.

Registry No. [(bpy)₂ClRu(4,4'-bpy)OsCl(bpy)₂](PF₆)₂, 91128-12-0; [(bpy)₂ClOs(4,4'-bpy)]PF₆, 91190-06-6; *cis*-(bpy)₂RuCl₂, 19542-80-4; [(bpy)₂Ru(bpm)](PF₆)₂, 65013-23-2; [(bpy)₂Ru(bpm)Ru(bpy)₂](PF₆)₄, 65013-25-4; [(bpy)₂Os(bpm)](PF₆)₂, 91157-03-8; *cis*-(bpy)₂OsCl₂, 79982-56-2; [(bpy)₂Ru(bpm)Os(bpy)₂](PF₆)₄, 91128-14-2; [(bpy)₂Ru(pyzc)]PF₆, 91128-16-4; [(bpy)₂ClRu(pyzc)Ru(bpy)₂](PF₆)₂, 91128-18-6; [(bpy)₂Os(pyzc)]PF₆, 91128-20-0; [(bpy)₂ClRu(pyzc)Os(bpy)₂](PF₆)₂, 91128-22-2; [(bpy)₂ClRu(pyzc)RuCl(bpy)₂](PF₆)₂, 91128-23-3; [(bpy)₂ClRu(pyzc)OsCl(bpy)₂](PF₆)₂, 91128-25-5; [(bpy)₂ClRu(4,4'-bpy)RuCl(bpy)₂](PF₆)₂, 49734-40-9; [(bpy)₂ClRu(pyzc)RuCl(bpy)₂](PF₆)₃, 91128-27-7; [(bpy)₂ClRu(pyzc)OsCl(bpy)₂](PF₆)₃, 91128-35-7; [(bpy)₂ClRu(4,4'-bpy)RuCl(bpy)₂](PF₆)₃, 91128-29-9; [(bpy)₂ClRu(4,4'-bpy)OsCl(bpy)₂](PF₆)₃, 91157-05-0; [(bpy)₂Ru(bpm)Ru(bpy)₂](PF₆)₅, 91128-31-3; [(bpy)₂Ru(bpm)Os(bpy)₂](PF₆)₅, 91128-37-9; [(bpy)₂ClRu(pyzc)Ru(bpy)₂](PF₆)₃, 91128-33-5; [(bpy)₂ClRu(pyzc)Os(bpy)₂](PF₆)₃, 91128-39-1.

Contribution from the Department of Chemistry, North Carolina State University, Raleigh, North Carolina 27650

Unique Redox and Spectroscopic Properties of Dipyrindylamine Complexes of d^6 Transition Metals: Electrochemical Behavior

DAVID E. MORRIS, YASUHIKO OHSAWA, DONALD P. SEGERS, M. KEITH DEARMOND,* and KENNETH W. HANCK*

Received November 2, 1983

Room- and low-temperature cyclic voltammetric and spectroscopic results in CH_3CN are presented for the series of complexes $[Ru(HDPA)_n(bpy)_{3-n}]^{2+}$ (**1**) ($n = 0-3$), $[Ru(DPA)_n(bpy)_{3-n}]^{(2-n)+}$ (**2**) ($n = 0-3$), and $[Ru(HDPA)_n(DPA)_{3-n}]^{(n-1)+}$ (**3**) ($n = 0-3$), where HDPA = di-2-pyrindylamine, DPA⁻ = deprotonated dipyrindylamine, and bpy = 2,2'-bipyridine. For **1** at -40 °C the voltammetric pattern reveals reversible reduction waves corresponding to the number of coordinated bpy ligands and one irreversible reduction wave for all HDPA-coordinated species at more negative potentials attributed to pyridyl π^* reduction. All species have one reversible oxidation wave corresponding to a metal-localized Ru(III/II) process. For **2** the reduction pattern still corresponds to reversible bpy reduction processes while there are no indications of reduction processes associated with DPA⁻. Most notable is the appearance of additional reversible oxidation waves in the potential region from -0.4 to +1.2 V (vs. $Fc^{+/0}$). Three such waves are seen for the $n = 2$ complex and two for $n = 1$. The most negative of these waves is shown from ESR results to correspond to a Ru(III/II) couple while the remaining waves involve further metal-localized oxidations and/or DPA⁻-localized oxidations. For **3** only irreversible reduction waves are seen at very negative potentials. Consistent with the other results is the appearance of an additional oxidation wave for **3** ($n = 2$). For **1** visible charge-transfer bands indicating transitions from Ru(II) to both the bpy π^* orbitals (~450 nm) and the HDPA pyridyl π^* orbitals (350 nm) are observed. The emission remains $d\pi^*$ from bpy as in the $n = 0$ complex. For **2** ($n = 1$ and 2) very low energy charge-transfer transitions (558 and 605 nm, respectively) assigned as $d\pi^*$ (bpy) are seen. The energies of these bands correlate well with the electrochemically predicted values. These results confirm that substantial changes occur in coordinated HDPA on deprotonation, and the results for **2** suggest that a metal-ligand interaction unique to Ru imine complexes exists.

Introduction

Recent photophysical, electrochemical, and electron spin resonance studies, by both these laboratories¹⁻⁹ and others,¹⁰⁻¹³ conclusively establish that for the majority of nominally d^6

transition-metal complexes of multidentate imine ligands such as $[Ru(bpy)_3]^{2+}$ the lowest excited-state orbital (the orbital from which $d\pi^*$ or $\pi\pi^*$ emission arises in spectroscopy and the redox orbital in electrochemistry) is localized on a single chelate ring (i.e. spatially isolated) with only minimal inter-ligand interaction. The cyclic voltammetric pattern is remarkably similar for all these complexes and has proven very useful in elucidating the single ring nature of the redox orbitals.^{3-6,8-10} For the iron group metal polypyridine complexes the voltammetry reveals only one oxidation wave assigned to a metal-localized M(III/II) couple whereas a series of reduction waves is observed in a pattern indicative of sequential addition of one electron into each of the lowest available diimine-localized π^* orbitals followed at more negative potentials by the addition of a second electron into each of these orbitals. With relatively few exceptions there are no intervening heterogeneous charge-transfer kinetic or chemical complications. Furthermore, the voltammetric results provide a valuable complement to the spectroscopic data and can assist in making spectroscopic assignments.¹⁴⁻¹⁶

- (1) DeArmond, M. K.; Carlin, C. M. *Coord. Chem. Rev.* **1981**, *36*, 325.
- (2) Carlin, C. M.; DeArmond, M. K. *Chem. Phys. Lett.* **1982**, *89*, 297.
- (3) Motten, A. G.; Hanck, K. W.; DeArmond, M. K. *Chem. Phys. Lett.* **1981**, *79*, 541.
- (4) Morris, D. E.; Hanck, K. W.; DeArmond, M. K. *J. Am. Chem. Soc.* **1983**, *105*, 3032.
- (5) Morris, D. E.; Hanck, K. W.; DeArmond, M. K. *J. Electroanal. Chem. Interfacial Electrochem.* **1983**, *149*, 115.
- (6) DeArmond, M. K.; Hanck, K. W.; Morris, D. E.; Ohsawa, Y.; Whitten, D. G.; Neveux, P. E. *J. Am. Chem. Soc.* **1983**, *105*, 6522.
- (7) Carlin, C. M.; DeArmond, M. K., to be submitted for publication in *J. Am. Chem. Soc.*
- (8) Kahl, J. L.; Hanck, K. W.; DeArmond, M. K. *J. Phys. Chem.* **1978**, *82*, 540.
- (9) Kahl, J. L.; Hanck, K. W.; DeArmond, M. K. *J. Phys. Chem.* **1979**, *83*, 2611.
- (10) Saji, T.; Aoyagui, S. *J. Electroanal. Chem. Interfacial Electrochem.* **1980**, *110*, 329 and references therein.
- (11) Heath, G. A.; Yellowlees, L. J.; Braterman, P. S. *Chem. Phys. Lett.* **1982**, *92*, 646.
- (12) Dallinger, R. F.; Woodruff, W. H. *J. Am. Chem. Soc.* **1979**, *101*, 4391.
- (13) Bradley, P. G.; Nurit, K.; Hornberger, B. A.; Dallinger, R. F.; Woodruff, W. H. *J. Am. Chem. Soc.* **1981**, *103*, 7441.

- (14) Rillema, D. P.; Allen, G.; Meyer, T. J.; Conrad, D. *Inorg. Chem.* **1983**, *22*, 1617.